Factors Associated With Dysfunction of Glymphatic System in Patients With Glioma

Cheng Hong Toh[1,2]* and Tiing Yee Siow[1]

[1] Department of Medical Imaging and Intervention, Chang Gung Memorial Hospital at Linkou, Tao-Yuan, Taiwan,
[2] Chang Gung University College of Medicine, Tao-Yuan, Taiwan

Objectives: Rodent experiments have provided some insights into the changes of glymphatic function associated with glioma growth. The diffusion tensor image analysis along the perivascular space (DTI-ALPS) method offers an opportunity for the noninvasive investigation of the glymphatic system in patients with glioma. We aimed to investigate the factors associated with glymphatic function changes in patients with glioma.

Materials and Methods: A total of 201 glioma patients (mean age = 47.4 years, 116 men; 86 grade II, 52 grade III, and 63 grade IV) who had preoperative diffusion tensor imaging for calculation of the ALPS index were retrospectively included. Information collected from each patient included sex, age, tumor grade, *isocitrate dehydrogenase 1* (*IDH1*) mutation status, peritumoral brain edema volume, tumor volume, and ALPS index. Group differences in the ALPS index according to sex, tumor grade, and *IDH1* mutation status were assessed using analysis of covariance with age adjustment. Linear regression analyses were performed to identify the factors associated with the ALPS index.

Results: Group comparisons revealed that the ALPS index of grade II/III gliomas was significantly higher than that of grade IV gliomas ($p < 0.001$). The ALPS index of *IDH1* mutant gliomas was significantly higher than that of *IDH1* wild-type gliomas ($p < 0.001$). On multivariable linear regression analysis, *IDH1* mutation ($\beta = 0.308$, $p < 0.001$) and peritumoral brain edema volume ($\beta = -0.353$, $p < 0.001$) were the two independent factors associated with the ALPS index.

Conclusion: *IDH1* wild-type gliomas and gliomas with larger peritumoral brain edema volumes were associated with a lower ALPS index, which may reflect impaired glymphatic function.

Keywords: glioma, glymphatic system, peritumoral brain edema, analysis along perivascular space (ALPS) index, diffusion tensor imaging

INTRODUCTION

The glymphatic system has been recently recognized as a pathway for waste clearance and maintaining fluid balance in the brain parenchymal interstitium (1). Cerebrospinal fluid (CSF) from the subarachnoid space flows into the brain parenchyma through periarterial spaces of the penetrating arteries and, under the influence of aquaporin-4 (AQP4) water channels, mixes with parenchymal

interstitial fluid. The interstitial fluid and its solutes then move into the perivenous and perineuronal spaces, thereafter leaving the brain parenchyma. The discovery of the glymphatic system led to a new perspective into the pathogenesis of brain diseases such as neurodegeneration (2) and acute ischemic infarct (3). Recent studies have shown that the glymphatic system may play an essential role in brain tumor immunity and might be targeted in brain tumor immunotherapy (4).

Rodent experiments have provided some insights into the changes of glymphatic function associated with glioma growth. In rodent studies, reduced CSF efflux rate (5) and remodeling of the glymphatic pathway (4) were observed in glioma-bearing mice, and these changes may be associated with the formation of peritumoral brain edema. Despite substantial knowledge having been gained from animal studies, further research is necessary to confirm whether the findings regarding the glymphatic system of animals apply to humans. Noninvasive approaches such as the morphological assessment of intracranial perivascular spaces with structural magnetic resonance imaging (MRI) (6–9) and measurement of water diffusivity using diffusion MRI (10–12) have been proposed for the evaluation of human glymphatic function.

The analysis along the perivascular space (ALPS) index (10) is a diffusion metric derived from diffusion tensor imaging (DTI). It is thought to reflect the diffusivity along the perivascular spaces of medullary veins at the level of the lateral ventricle body and, thus, may serve as an estimate of human glymphatic function. Alterations of the ALPS index correlate with the Mini-Mental State Examination scores in patients with Alzheimer's disease and are thought to reflect glymphatic dysfunction. The ALPS index is also significantly lower in normal pressure hydrocephalus patients and points toward glymphatic dysfunction, as indicated by delayed clearance of intrathecally injected gadobutrol (13, 14).

The ALPS index offers an opportunity for the noninvasive investigation of the human glymphatic system. Thus, we took advantage of this method to evaluate the glymphatic system in patients with glioma. We aimed to investigate the correlations of glymphatic function with the volumes of tumor and peritumoral brain edema, tumor grades, and *isocitrate dehydrogenase 1* (*IDH1*) mutation status.

MATERIALS AND METHODS

Study Subjects
Approval for reviewing patients' clinical data and preoperative MRI studies was obtained from our Institutional Review Board. Between 2008 and 2018, a total of 239 consecutive patients with a histopathological diagnosis of grade II, III, or IV glioma underwent preoperative DTI at our institution. A total of 38 patients were excluded due to age younger than 18 years ($n = 2$), motion artifacts ($n = 3$), tumors limited to the infratentorial compartment ($n = 4$), and the *IDH1* mutation status not being available ($n = 29$). Thus, a total of 201 patients (85 women and 116 men, mean age = 47.4 ± 15.5 years, range = 18–91 years) were analyzed. None of the patients had begun corticosteroid treatment, radiation therapy, chemotherapy, or had previous brain surgery at the time of their MRI studies.

Clinical and Imaging Information
Patients' medical records and MRI studies were retrospectively reviewed to collect information including sex, age, tumor grade, and tumor *IDH1* mutation status. Histopathological diagnosis was made by a board-certified neuropathologist with 20 years of experience according to the 2007 WHO classification of central nervous system tumors before 2016 and thereafter based on the 2016 WHO classification.

MRI
All MRI studies were performed using a 3-T unit (Magnetom Tim Trio, Siemens, Erlangen, Germany) with a 12-channel phased-array head coil. All examinations included T2-weighted, susceptibility-weighted, DTI, and T1-weighted sequences acquired in the transverse plane before and after administration of 0.1 mmol/kg body weight gadopentetate dimeglumine (Magnevist; Schering, Berlin, Germany).

DTI was performed using a single-shot echo planar sequence (EPI) with the following parameters: repetition time/echo time (TR/TE), 5,800/83 ms; diffusion gradient encoding in 20 directions; $b = 0, 1,000 \text{ s/mm}^2$; field of view (FOV), 256 × 256 mm; matrix size, 128 × 128; section thickness, 2 mm; and number of signals acquired, 4. A total of 50–60 sections without intersection gaps were used to cover the cerebral hemispheres, brainstem, and the cerebellum. Generalized autocalibrating partially parallel acquisitions (GRAPPA) with a reduction factor set at 2 were used during DTI acquisitions. Contrast-enhanced T1-weighted images [TR/TE = 2,000/2.63 ms, section thickness = 1 mm, inversion time (TI) = 900 ms, acquisition matrix = 224 × 256, and FOV = 224 × 256 mm] were acquired after completion of the DTI sequence.

Image Post-Processing and Analysis
The software nordicICE (nordic Image Control and Evaluation, version 2; Nordic Imaging Lab, Bergen, Norway) was used for all volume measurements. All images of each patient were co-registered based on a 3D non-rigid transformation and mutual information. The adequacy of registration was visually assessed and manual adjustments were performed by changing the transformation parameters of translation, rotation, and/or scaling, as necessary. The ALPS index was measured with 3D Slicer, version 4.10.2 (http://www.slicer.org). Blinded to histopathologic diagnoses, two neuroradiologists (with 16 and 6 years of experience) independently performed all measurements. If the tumors were found in both hemispheres, only those in the hemisphere with the larger tumor were selected for measurements of volumes. If multiple tumors or peritumoral brain edema areas were present, all were included as long as their sizes were larger than $1 \times 1 \text{ cm}^2$.

Measurements of Volumes of Peritumoral Brain Edema, Whole Tumor, Enhancing Tumor Portions, Non-Enhancing Tumor Portions, Necrotic Portions, and Hemorrhagic Portions
One polygonal region of interest (ROI) was first placed on each T2-weighted image to include the entire peritumoral brain edema and

tumor, followed by another ROI drawn to include the entire tumor on each contrast-enhanced T1-weighted image. Subtracting the second ROI from the first ROI yielded the isolated peritumoral brain edema area. If non-enhancing, necrotic, and hemorrhagic tumor portions were present, they were measured by placing the ROIs on T2-weighted or contrast-enhanced T1-weighted images with reference to other pulse sequence images. In all the slices covering the whole tumor, the ROIs were drawn. Non-enhancing tumor portions were tumor components that showed T2-weighted/fluid-attenuated inversion recover (FLAIR) hyperintensity with corresponding T1-weighted hypointensity and no contrast enhancement. Necrotic tumor portions were tumor components that demonstrated central T2-weighted hyperintensity (i.e., fluid) with surrounding contrast enhancement. Hemorrhagic tumor portions were tumor components that had T1-weighted hyperintensity, T2-weighted hypointensity, or susceptibility-weighted hypointensity. Subtracting the ROIs of the non-enhancing, necrotic, and hemorrhagic tumor portions from the tumor ROI yielded the enhancing tumor area. The slice volume of each ROI was computed by multiplying the area by slice distance (slice thickness + slice gap). The total volumes of the peritumoral brain edema, whole tumor, enhancing tumor portion, non-enhancing tumor portion, necrotic portion, and hemorrhagic portion were calculated by summing up all the slice volumes. An example of ROI segmentation is shown in **Figure 1**.

Measurement of the ALPS Index

The diffusion tensor image analysis along the perivascular space (DTI-ALPS) method (10) was used to evaluate the glymphatic function. This method evaluates the diffusivity along with the perivascular space on a transverse slice at the level of the lateral ventricle body. The medullary veins, accompanied by their perivascular spaces, run perpendicular to the ventricular walls at the level of the lateral ventricular bodies in a right–left or a left–right direction (i.e., x-axis in the image coordinate). In this level, the corticofugal corona radiata projection fibers run in the craniocaudal direction (i.e., z-axis in the image coordinate)

adjacent to the lateral ventricles. The superior longitudinal fascicle, which represents the association fibers, runs in the anterior–posterior direction (i.e., y-axis in the image coordinate) and is located lateral to the corona radiata. As the perivascular space is nearly perpendicular to both the projection fibers and association fibers, the mean x-axis diffusivity in both fibers (D_{xproj} and D_{xassoc} for x-axis diffusivity in the projection fiber and the association fiber, respectively) can reflect the change in perivascular flow, after being normalized to the mean diffusivity that is perpendicular to the x-axis and to the direction of the fiber tracts (y-axis for the projection fiber, where the diffusivity is denoted as D_{yproj}; z-axis for the association fiber, where the diffusivity is denoted as D_{zassoc}). To estimate the glymphatic activity, the ALPS index is defined as follows:

$$\text{ALPS index} = \frac{\text{mean}(D_{xproj}, D_{xassoc})}{\text{mean}(D_{yproj}, D_{zassoc})} \quad (1)$$

Diffusion metric images were generated by using 3D Slicer, version 4.10.2 (http://www.slicer.org). The diffusion tensor is calculated based on the "Diffusion Tensor Estimated function" in 3D Slicer. Dxx, Dyy, and Dzz were extracted from the tensor data using a self-written Python script in the 3D Slicer Python interactor. The ROIs of the projection (mean size = 35 ± 19 mm^2) and association fibers (mean size = 30 ± 18 mm^2) ipsilateral to the tumors were drawn on a slice at the level of the lateral ventricular body based on a directionality encoded map. The ALPS index was computed according to Equation 1 above. An example of ROI placement for ALPS index measurement is shown in **Figure 1**.

Statistical Analysis

A commercially available statistical software package (SPSS 22; IBM, Armonk, NY, USA) was used for analysis, and p-values <0.05 were considered to indicate a statistical significance. Continuous variables are denoted as the mean ± standard deviation, unless otherwise noted. The Kolmogorov–Smirnov test was used to assess the normality of continuous variables.
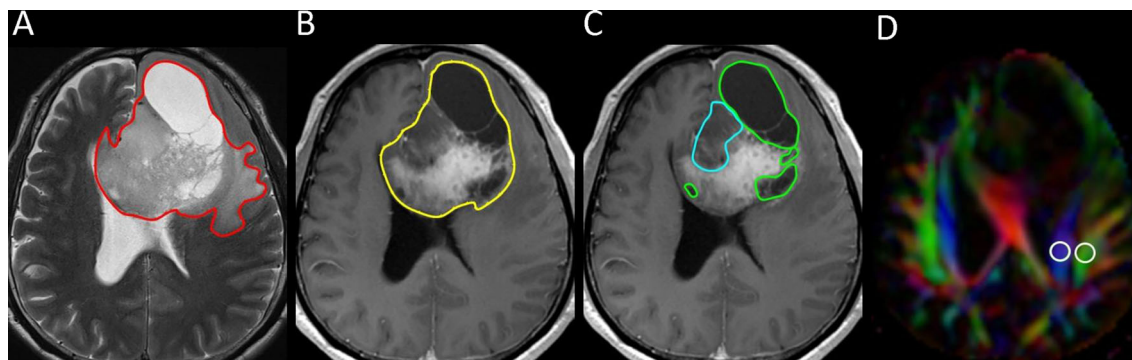
FIGURE 1 | Example of how regions of interest (ROIs) were segmented in a left frontal grade II glioma. **(A)** Transverse T2-weigthed image showing a manually drawn polygonal ROI (*red*) that includes the entire peritumoral brain edema and the whole tumor. **(B, C)** On contrast-enhanced T1-weighted images, the ROIs of whole tumor (*yellow*), non-enhancing tumor (*blue*), and necrotic portion (*green*) are shown. **(D)** Directionally encoded color map illustrating the ROIs of the projection (*blue area*) and association (*green area*) fibers in the left periventricular region for calculation of the analysis along the perivascular space (ALPS) index.

Variance inflation factors were used to detect multicollinearity. Interobserver variability in the measurements of volumes and the ALPS index was assessed by intraclass correlation coefficients (ICCs) with 95% confidence intervals (CIs) based on an absolute-agreement, two-way random-effects model. The final values of all measurements were obtained by taking the mean of the two observers' independent measurements.

Group differences in the ALPS index according to sex (man vs. woman), tumor grade (grade II vs. III vs. IV), and IDH1 mutation status (mutant vs. wild-type) were assessed using analysis of covariance with age adjustment (15, 16). Additional Bonferroni correction was performed for tumor grade.

The associations of ALPS index with age, sex, histological grade, IDH1 mutation status, whole tumor volume, enhancing tumor volume, non-enhancing tumor volume, necrotic portion volume, and hemorrhagic portion volume were first analyzed with univariable linear regression. All variables were entered as potential covariates in the stepwise multivariable linear regression analysis to identify independent factors associated with the ALPS index.

RESULTS

Table 1 summarizes the patients' characteristics and all measurements. Among the 201 patients with gliomas, 86 had grade II, 52 had grade III, and 63 had grade IV. A total of 107 (53.2%) tumors were IDH1-mutant. Eighty-four (41.8%) patients had glioma involving the right cerebral hemisphere.

There were excellent interobserver agreements (ICC = 0.822–0.948, $p < 0.001$) in the measurements of peritumoral brain edema volumes, whole tumor volumes, enhancing tumor volumes, non-enhancing tumor volumes, necrotic portions volumes, hemorrhagic portions volumes, and the ALPS index. The mean volumes (in cubic centimeters) of the peritumoral brain edema, whole tumor, enhancing tumor, non-enhancing tumor, necrotic portion, and hemorrhagic portion were 26.09 ± 30.38, 53.47 ± 39.40, 16.34 ± 18.58, 29.84 ± 38.25, 5.78 ± 14.65, and 3.82 ± 11.91, respectively. The mean ALPS index for grade II, grade III, and grade IV gliomas were 1.454 ± 0.186, 1.421 ± 0.214, and 1.220 ± 0.112, respectively.

The results of ALPS index comparisons according to sex, tumor grade, and IDH1 mutation status with age adjustment are summarized in **Table 2**. The ALPS index of women was not significantly different from that of men ($p = 0.098$). The ALPS index of grade II and grade III gliomas was significantly higher than that of grade IV gliomas ($p < 0.001$). However, the ALPS index was not different between grade II and III gliomas ($p = 0.670$). The ALPS index of IDH1 wild-type gliomas was significantly lower than that of IDH1 mutant gliomas ($p < 0.001$). **Figure 2** shows the differences in the ALPS index according to sex, tumor grade, and IDH1 mutation status.

The results of linear regression analyses of the factors associated with the ALPS index are summarized in **Table 3**. On univariable linear regression analysis, the ALPS index correlated with age ($\beta = -0.147$, $p = 0.038$), sex ($\beta = -0.139$, $p = 0.049$), tumor grade ($\beta = -0.361$, $p < 0.001$), IDH1 mutation ($\beta = 0.384$, $p < 0.001$), peritumoral brain edema volume ($\beta = -0.439$, $p < 0.001$), enhancing tumor volume ($\beta = -0.348$, $p < 0.001$), and non-enhancing tumor volume ($\beta = 0.307$, $p < 0.001$). The associations of the ALPS index with whole tumor volume ($\beta = 0.101$, $p = 0.155$), necrotic portion volume ($\beta = -0.058$, $p = 0.410$), and hemorrhagic portion volume ($\beta = 0.002$, $p = 0.983$) were not statistically significant. **Figure 3** illustrates the correlations of the ALPS index with age, peritumoral brain edema volume, enhancing tumor volume, and non-enhancing tumor volume.

On stepwise multivariable linear regression analysis, IDH1 mutation ($\beta = 0.308$; $p < 0.001$) and peritumoral brain edema volume ($\beta = -0.353$; $p < 0.001$) were the two independent factors associated with the ALPS index. A lower ALPS index was associated with IDH1 wild-type gliomas and larger peritumoral brain edema volume.

TABLE 1 | Patient characteristics and all measurements.

| Characteristics	Grade II	Grade III	Grade IV	All
No. of patients	86	52	63	201
Mean age ± SD (years)	41.4 ± 13.3	45.2 ± 13.6	57.5 ± 15.1	47.4 ± 15.5
Sex				
Woman	41	23	21	85
Man	45	29	42	116
Tumor location				
Right cerebral	37	16	31	84
Left cerebral	49	36	32	117
IDH1 mutation				
Wild-type	20	18	56	94
Mutant	66	34	7	107
Peritumoral edema volume (cm^3)	13.81 ± 18.36	17.04 ± 21.11	50.33 ± 35.70	26.09 ± 30.38
Whole tumor volume (cm^3)	52.82 ± 45.56	58.69 ± 40.92	50.04 ± 27.35	53.47 ± 39.40
Enhancing tumor volume (cm^3)	1.59 ± 6.21	12.27 ± 19.26	31.22 ± 15.46	16.34 ± 18.58
Non-enhancing tumor volume (cm^3)	47.02 ± 42.57	33.11 ± 30.57	3.69 ± 18.75	29.84 ± 38.25
Necrotic portion volume (cm^3)	1.94 ± 7.30	9.34 ± 22.39	8.10 ± 13.05	5.78 ± 14.65
Hemorrhagic portion volume (cm^3)	1.18 ± 10.95	3.05 ± 11.43	8.06 ± 12.55	3.82 ± 11.91
ALPS index	1.454 ± 0.186	1.421 ± 0.214	1.220 ± 0.112	1.372 ± 0.202

Except where indicated, data are numbers of patients.
SD, standard deviation; ALPS, analysis along the perivascular space.

TABLE 2 | Comparisons of the ALPS index according to sex, tumor grade, and *IDH1* mutation status with age adjustment.

Characteristics	ALPS index	Pairwise comparison	*p*-value	95% CI
Sex		Woman *vs.* man	0.098	−0.009 to 0.105
Woman	1.405 ± 0.216			
Man	1.348 ± 0.190			
Tumor grade		Grade II *vs.* III	0.670	−0.037 to 0.112
Grade II	1.454 ± 0.186	Grade II *vs.* IV	<0.001	0.178–0.333
Grade III	1.421 ± 0.214	Grade III *vs.* IV	<0.001	0.135–0.301
Grade IV	1.220 ± 0.112			
IDH1 mutation		Wild-type *vs.* mutant	<0.001	−0.235 to −0.097
Wild-type	1.311 ± 0.151			
Mutant	1.466 ± 0.201			

Data are the mean ± SD.
CI, confidence interval; ALPS, analysis along the perivascular space.
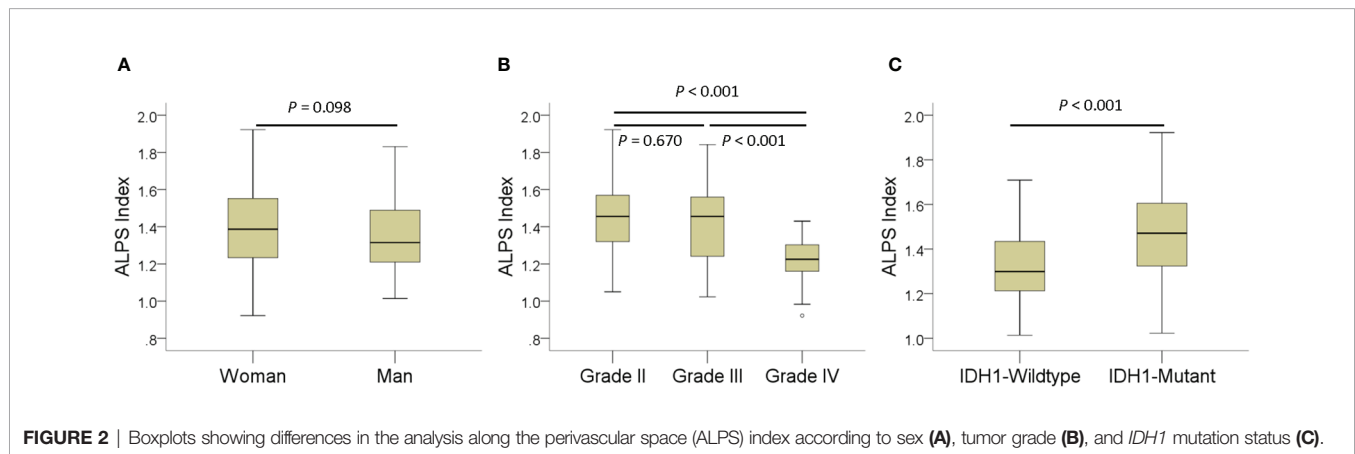
FIGURE 2 | Boxplots showing differences in the analysis along the perivascular space (ALPS) index according to sex **(A)**, tumor grade **(B)**, and *IDH1* mutation status **(C)**.

DISCUSSION

In the present study, the *IDH1* mutation status of gliomas and the peritumoral brain edema volume were two independent factors associated with the ALPS index. As reflected by a lower ALPS index, glymphatic function was impaired in *IDH1* wild-type gliomas and gliomas associated with larger peritumoral brain edema volumes. To our knowledge, this is the first study of human glymphatic function in patients with glioma.

The inverse correlation between the ALPS index and peritumoral brain edema volume was observed in meningiomas (17). It was proposed that tumor growth disrupts the balance between periarterial CSF influx and perivenous interstitial fluid efflux and results in the accumulation of interstitial fluid, i.e., peritumoral brain edema. A higher glymphatic function may facilitate interstitial fluid clearance and reduce or even prevent edema. In contrast, insufficient glymphatic function for interstitial fluid clearance may contribute to edema formation. Therefore, glymphatic dysfunction may explain the pathogenesis of peritumoral brain edema in meningiomas, which are extra-axial and have no direct contact with the brain interstitium.

The pathogenesis of peritumoral brain edema in gliomas is traditionally thought to represent the net transport of fluid from the intravascular compartment into the brain interstitium due to the proliferation of microvessels that have defects in their inter-

endothelial tight junctions (18). However, this theory does not explain the formation of peritumoral brain edema in low-grade gliomas with intact tight junctions (19, 20). In our study, we also observed an inverse relationship between the ALPS index and peritumoral brain edema volume. This finding suggests that the peritumoral brain edema associated with intra-axial tumors (i.e., gliomas) may also be related to glymphatic dysfunction.
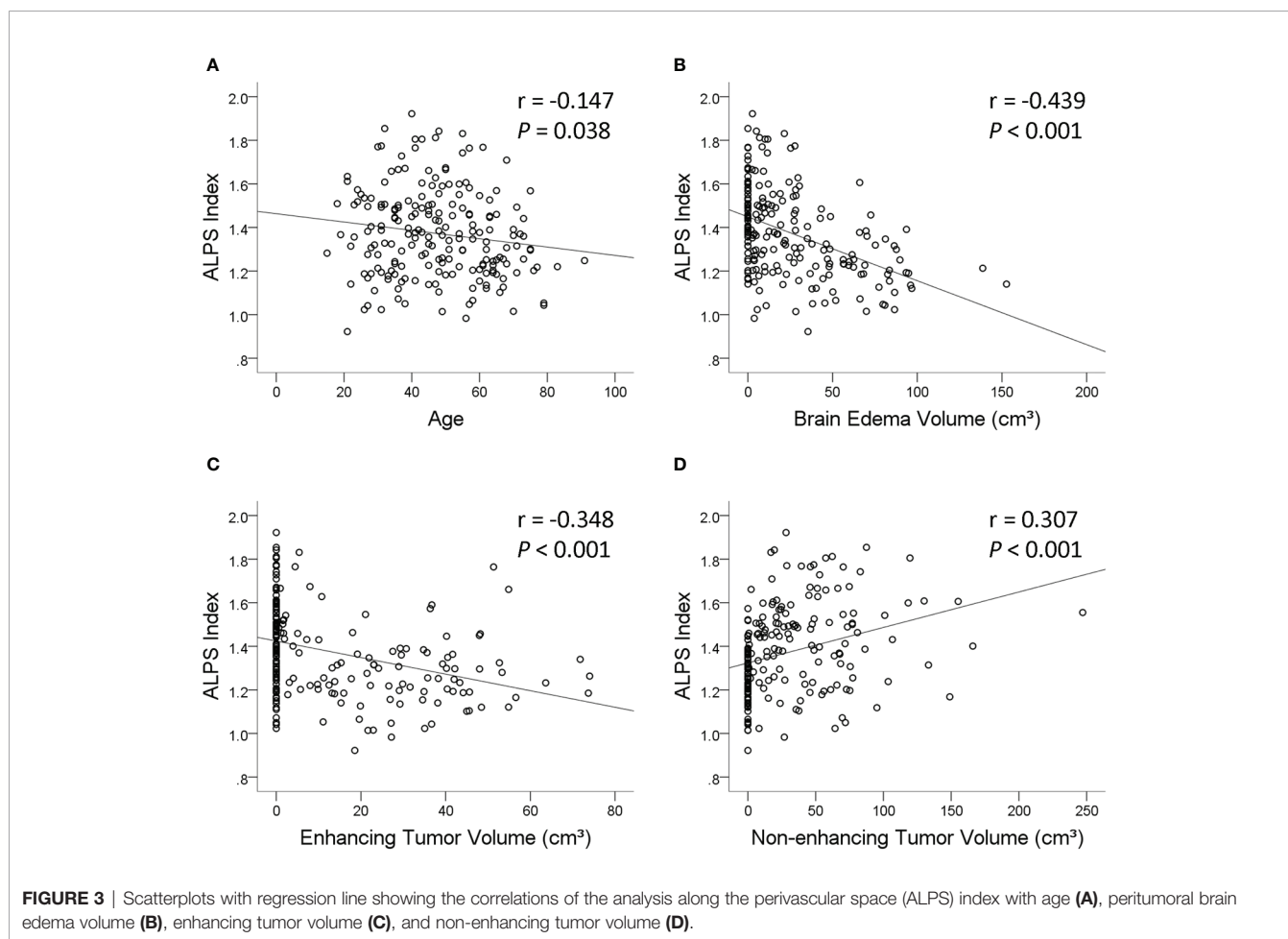
A recent study has shown that changes in the supporting structures of the blood–brain barrier, such as astrocytes, pericytes, and microglial cells, may also be associated with the influx of fluid into the brain interstitium (21). The astrocyte covering of brain microvessels seems to be rate limiting to water movement (21), and AQP4 water channels located on astrocytic foot processes may play a significant role in peritumoral brain edema formation. A strong correlation between peritumoral brain edema and upregulated astrocyte AQP4 expression in human gliomas suggests that increased AQP4 expression may be essential to the pathogenesis of peritumoral brain edema (22). Since AQP4 water channels are part of the glymphatic system, we speculate that there may an association between the ALPS index and the expression of AQP4 water channels. Further studies are needed to establish the role of the ALPS index as an imaging marker of AQP4 expression in gliomas.

The changes of glymphatic function associated with glioma growth have only been investigated in a few animal studies. In a study using an orthotopic xenograft glioma model (5), glioma

TABLE 3 | Univariable and multivariable linear regression analyses of factors associated with the ALPS index.

Characteristics	ALPS Index			
	Univariate linear regression		Multivariate linear regression	
	β	*p*-value	β	*p*-value
Age (years)	−0.147	0.038	0.075	0.351
Sex	−0.139	0.049	0.001	0.993
Tumor grade	−0.361	<0.001	−0.127	0.149
IDH1 mutation	0.384	<0.001	0.308	<0.001
Brain edema volume	−0.439	<0.001	−0.353	<0.001
Whole tumor volume	0.101	0.155	0.119	0.122
Enhancing tumor volume	−0.348	<0.001	0.024	0.778
Non-enhancing tumor volume	0.307	<0.001	0.108	0.187
Necrotic portion volume	−0.058	0.410	−0.033	0.653
Hemorrhagic portion volume	0.064	0.454	0.133	0.092

ALPS, analysis along the perivascular space; β, standardized coefficient.

FIGURE 3 | Scatterplots with regression line showing the correlations of the analysis along the perivascular space (ALPS) index with age **(A)**, peritumoral brain edema volume **(B)**, enhancing tumor volume **(C)**, and non-enhancing tumor volume **(D)**.

growth caused glymphatic dysfunction with reduced CSF flow to the extracranial space. In our study, the glymphatic function of *IDH1* wild-type gliomas, measured with the ALPS index, was significantly lower than that of *IDH1* mutant gliomas. To the best of our knowledge, no human studies have reported the association between glymphatic function and the *IDH1* mutation status of gliomas.

IDH1 wild-type gliomas are known to behave more aggressively than *IDH1* mutant gliomas (23). We speculate that the spread of *IDH1* wild-type gliomas is associated with greater disruption to the flow of interstitial fluid and, consequently, lower glymphatic function. Alternatively, tumor-associated glymphatic pathway remodeling may be responsible for the differences in glymphatic function between *IDH1* wild-type and *IDH1* mutant gliomas. In mice

harboring gliomas, glymphatic function is increased for waste and fluid clearance by extensive growth of meningeal lymphatic vessels, which are downstream of the glymphatic pathway (4). A previous study showed that the growth of glioblastomas (mostly *IDH1* wild-type) from small to large tumors could take as short as 1.5 months (24). In contrast, *IDH1* mutant gliomas are known for longer survival and may be stable for years (25). We therefore speculate that the lower glymphatic function of *IDH1* wild-type gliomas may be related to their short duration of tumor growth, which does not allow extensive remodeling of the glymphatic pathway.

Although the mechanism for the association between glymphatic function and *IDH1* mutation status is unclear, the relationship has revealed some potential utilities for the ALPS index. Many MR imaging markers have been found to be useful in predicting the *IDH1* mutation status in gliomas (26–29). However, most of them are measured in the tumors, but may not be feasible when a large hemorrhage or necrosis is present. In contrast, the ALPS index is measured in the periventricular region outside of the tumor and, thus, may serve as an alternative marker for *IDH1* mutation prediction. Besides, the ALPS index may also be a prognostic factor for patient survival due to its correlation with *IDH1* mutation status. Further studies are needed to establish the predictive and prognostic roles of the ALPS index.

The anatomical relationship of the perivascular spaces, projection fibers, and association fibers in the periventricular region is the theoretical basis of the DTI-ALPS method. Although this method is based on a deductive model, it is frequently used to investigate human glymphatic function. Its potential to serve as an imaging marker of glymphatic activity has been reported in many clinical conditions such as Alzheimer's disease (10, 30), normal pressure hydrocephalus (31, 32), Parkinson disease (33, 34), age-related iron deposition (15), diabetic cognitive impairment (35), and meningioma-associated brain edema (17). However, there are limitations to this method and, consequently, our study. Firstly, the diffusion signal measured in clinical settings reflects overall changes in water mobility associated with many processes occurring at scales much smaller than typical MRI voxels. Therefore, we cannot definitely state that the ALPS index is a measure of glymphatic function. Secondly, the ALPS index could only measure the perivascular water flow that runs in a right-to-left direction and in the periventricular region. Further studies are needed to establish its correlation with overall glymphatic function. Finally, our study is a snapshot in time and does not include longitudinal data on temporal changes of the ALPS index and peritumoral brain edema volume following treatment. These

pieces of information would be helpful to further establish the role of the glymphatic system in brain edema formation.

CONCLUSIONS

In conclusion, *IDH1* wild-type gliomas and gliomas with larger peritumoral brain edema volumes were associated with a lower ALPS index, which may reflect an impaired glymphatic function. The lower ALPS index in *IDH1* wild-type gliomas may suggest an association between glymphatic dysfunction and tumor aggressiveness. In addition, the correlation between larger peritumoral brain edema volumes and a lower ALPS index suggests that the formation of peritumoral brain edema may be related to glymphatic dysfunction.

DATA AVAILABILITY STATEMENT

The raw data supporting the conclusions of this article will be made available by the authors, without undue reservation.

ETHICS STATEMENT

The studies involving human participants were reviewed and approved by Chang Gung Medical Foundation Institutional Review Board. Written informed consent for participation was not required for this study in accordance with the national legislation and the institutional requirements.

AUTHOR CONTRIBUTIONS

CT and TS contributed to the conception and design of the study and to the acquisition and analysis of data. CT drafted the text, prepared the figures, and wrote the first draft of the manuscript. All authors read the final manuscript. All authors contributed to the article and approved the submitted version.

FUNDING

REFERENCES

1. Rasmussen MK, Mestre H, Nedergaard M. The Glymphatic Pathway in Neurological Disorders. *Lancet Neurol* (2018) 17(11):1016–24. doi: 10.1016/s1474-4422(18)30318-1
2. Nedergaard M, Goldman SA. Glymphatic Failure as a Final Common Pathway to Dementia. *Science* (2020) 370(6512):50–6. doi: 10.1126/science.abb8739
3. Mestre H, Du T, Sweeney AM, Liu G, Samson AJ, Peng W, et al. Cerebrospinal Fluid Influx Drives Acute Ischemic Tissue Swelling. *Science* (2020) 367(6483):eaax7171. doi: 10.1126/science.aax7171

4. Hu X, Deng Q, Ma L, Li Q, Chen Y, Liao Y, et al. Meningeal Lymphatic Vessels Regulate Brain Tumor Drainage and Immunity. *Cell Res* (2020) 30(3):229–43. doi: 10.1038/s41422-020-0287-8
5. Ma Q, Schlegel F, Bachmann SB, Schneider H, Decker Y, Rudin M, et al. Lymphatic Outflow of Cerebrospinal Fluid Is Reduced in Glioma. *Sci Rep* (2019) 9(1):14815. doi: 10.1038/s41598-019-51373-9
6. Ballerini L, Lovreglio R, Valdés Hernández MDC, Ramirez J, MacIntosh BJ, Black SE, et al. Perivascular Spaces Segmentation in Brain MRI Using Optimal 3d Filtering. *Sci Rep* (2018) 8(1):2132. doi: 10.1038/s41598-018-19781-5
7. Sepehrband F, Barisano G, Sheikh-Bahaei N, Cabeen RP, Choupan J, Law M, et al. Image Processing Approaches to Enhance Perivascular Space Visibility

and Quantification Using MRI. *Sci Rep* (2019) 9(1):12351. doi: 10.1038/s41598-019-48910-x

8. Zong X, Lian C, Jimenez J, Yamashita K, Shen D, Lin W. Morphology of Perivascular Spaces and Enclosed Blood Vessels in Young to Middle-Aged Healthy Adults at 7T: Dependences on Age, Brain Region, and Breathing Gas. *Neuroimage* (2020) 218:116978. doi: 10.1016/j.neuroimage.2020.116978

9. Barisano G, Sheikh-Bahaei N, Law M, Toga AW, Sepehrband F. Body Mass Index, Time of Day and Genetics Affect Perivascular Spaces in the White Matter. *J Cereb Blood Flow Metab* (2021) 41(7):1563–78. doi: 10.1177/0271678x20972856

10. Taoka T, Masutani Y, Kawai H, Nakane T, Matsuoka K, Yasuno F, et al. Evaluation of Glymphatic System Activity With the Diffusion MR Technique: Diffusion Tensor Image Analysis Along the Perivascular Space (DTI-ALPS) in Alzheimer's Disease Cases. *Jpn J Radiol* (2017) 35(4):172–8. doi: 10.1007/s11604-017-0617-z

11. Harrison IF, Siow B, Akilo AB, Evans PG, Ismail O, Ohene Y, et al. Non-Invasive Imaging of CSF-Mediated Brain Clearance Pathways *via* Assessment of Perivascular Fluid Movement With Diffusion Tensor MRI. *Elife* (2018) 7:e34028. doi: 10.7554/eLife.34028

12. Debacker C, Djemai B, Ciobanu L, Tsurugizawa T, Le Bihan D. Diffusion MRI Reveals *In Vivo* and Non-Invasively Changes in Astrocyte Function Induced by an Aquaporin-4 Inhibitor. *PloS One* (2020) 15(5):e0229702. doi: 10.1371/journal.pone.0229702

13. Ringstad G, Vatnehol SAS, Eide PK. Glymphatic MRI in Idiopathic Normal Pressure Hydrocephalus. *Brain* (2017) 140(10):2691–705. doi: 10.1093/brain/awx191

14. Eide PK, Ringstad G. Delayed Clearance of Cerebrospinal Fluid Tracer From Entorhinal Cortex in Idiopathic Normal Pressure Hydrocephalus: A Glymphatic Magnetic Resonance Imaging Study. *J Cereb Blood Flow Metab* (2019) 39(7):1355–68. doi: 10.1177/0271678x18760974

15. Zhou W, Shen B, Shen WQ, Chen H, Zheng YF, Fei JJ. Dysfunction of the Glymphatic System Might Be Related to Iron Deposition in the Normal Aging Brain. *Front Aging Neurosci* (2020) 12:559603. doi: 10.3389/fnagi.2020.559603

16. Zhang Y, Zhang R, Ye Y, Wang S, Jiaerken Y, Hong H, et al. The Influence of Demographics and Vascular Risk Factors on Glymphatic Function Measured by Diffusion Along Perivascular Space. *Front Aging Neurosci* (2021) 13:693787. doi: 10.3389/fnagi.2021.693787

17. Toh CH, Siow TY, Castillo M. Peritumoral Brain Edema in Meningiomas May Be Related to Glymphatic Dysfunction. *Front Neurosci* (2021) 15:674898. doi: 10.3389/fnins.2021.674898

18. Stummer W. Mechanisms of Tumor-Related Brain Edema. *Neurosurg Focus* (2007) 22(5):E8. doi: 10.3171/foc.2007.22.5.9

19. Belykh E, Shaffer KV, Lin C, Byvaltsev VA, Preul MC, Chen L. Blood-Brain Barrier, Blood-Brain Tumor Barrier, and Fluorescence-Guided Neurosurgical Oncology: Delivering Optical Labels to Brain Tumors. *Front Oncol* (2020) 10:739. doi: 10.3389/fonc.2020.00739

20. Nduom EK, Yang C, Merrill MJ, Zhuang Z, Lonser RR. Characterization of the Blood-Brain Barrier of Metastatic and Primary Malignant Neoplasms. *J Neurosurg* (2013) 119(2):427–33. doi: 10.3171/2013.3.jns122226

21. Haj-Yasein NN, Vindedal GF, Eilert-Olsen M, Gundersen GA, Skare Ø, Laake P, et al. Glial-Conditional Deletion of Aquaporin-4 (Aqp4) Reduces Blood-Brain Water Uptake and Confers Barrier Function on Perivascular Astrocyte Endfeet. *Proc Natl Acad Sci USA* (2011) 108(43):17815–20. doi: 10.1073/pnas.1110655108

22. Saadoun S, Papadopoulos MC, Davies DC, Krishna S, Bell BA. Aquaporin-4 Expression Is Increased in Oedematous Human Brain Tumours. *J Neurol Neurosurg Psychiatry* (2002) 72(2):262–5. doi: 10.1136/jnnp.72.2.262

23. Louis DN, Wesseling P, Aldape K, Brat DJ, Capper D, Cree IA, et al. cIMPACT-NOW Update 6: New Entity and Diagnostic Principle Recommendations of the cIMPACT-Utrecht Meeting on Future CNS Tumor Classification and Grading. *Brain Pathol* (2020) 30(4):844–56. doi: 10.1111/bpa.12832

24. Toh CH, Castillo M. Early-Stage Glioblastomas: MR Imaging-Based Classification and Imaging Evidence of Progressive Growth. *AJNR Am J Neuroradiol* (2017) 38(2):288–93. doi: 10.3174/ajnr.A5015

25. Toh CH, Castillo M, Wei KC, Chen PY. MRS as an Aid to Diagnose Malignant Transformation in Low-Grade Gliomas With Increasing Contrast Enhancement. *AJNR Am J Neuroradiol* (2020) 41(9):1592–8. doi: 10.3174/ajnr.A6688

26. Kim M, Jung SY, Park JE, Jo Y, Park SY, Nam SJ, et al. Diffusion- and Perfusion-Weighted MRI Radiomics Model may Predict Isocitrate Dehydrogenase (IDH) Mutation and Tumor Aggressiveness in Diffuse Lower Grade Glioma. *Eur Radiol* (2020) 30(4):2142–51. doi: 10.1007/s00330-019-06548-3

27. Leather T, Jenkinson MD, Das K, Poptani H. Magnetic Resonance Spectroscopy for Detection of 2-Hydroxyglutarate as a Biomarker for IDH Mutation in Gliomas. *Metabolites* (2017) 7(2):29. doi: 10.3390/metabo7020029

28. Choi KS, Choi SH, Jeong B. Prediction of IDH Genotype in Gliomas With Dynamic Susceptibility Contrast Perfusion MR Imaging Using an Explainable Recurrent Neural Network. *Neuro Oncol* (2019) 21(9):1197–209. doi: 10.1093/neuonc/noz095

29. Thust SC, Hassanein S, Bisdas S, Rees JH, Hyare H, Maynard JA, et al. Apparent Diffusion Coefficient for Molecular Subtyping of Non-Gadolinium-Enhancing WHO Grade II/III Glioma: Volumetric Segmentation Versus Two-Dimensional Region of Interest Analysis. *Eur Radiol* (2018) 28(9):3779–88. doi: 10.1007/s00330-018-5351-0

30. Steward CE, Venkatraman VK, Lui E, Malpas CB, Ellis KA, Cyarto EV, et al. Assessment of the DTI-ALPS Parameter Along the Perivascular Space in Older Adults at Risk of Dementia. *J Neuroimaging* (2021) 31(3):569–78. doi: 10.1111/jon.12837\

31. Yokota H, Vijayasarathi A, Cekic M, Hirata Y, Linetsky M, Ho M, et al. Diagnostic Performance of Glymphatic System Evaluation Using Diffusion Tensor Imaging in Idiopathic Normal Pressure Hydrocephalus and Mimickers. *Curr Gerontol Geriatr Res* (2019) 2019:5675014. doi: 10.1155/2019/5675014

32. Bae YJ, Choi BS, Kim JM, Choi JH, Cho SJ, Kim JH. Altered Glymphatic System in Idiopathic Normal Pressure Hydrocephalus. *Parkinsonism Relat Disord* (2021) 82:56–60. doi: 10.1016/j.parkreldis.2020.11.009

33. Chen HL, Chen PC, Lu CH, Tsai NW, Yu CC, Chou KH, et al. Associations Among Cognitive Functions, Plasma DNA, and Diffusion Tensor Image Along the Perivascular Space (DTI-ALPS) in Patients With Parkinson's Disease. *Oxid Med Cell Longev* (2021) 2021:4034509. doi: 10.1155/2021/4034509

34. McKnight CD, Trujillo P, Lopez AM, Petersen K, Considine C, Lin YC, et al. Diffusion Along Perivascular Spaces Reveals Evidence Supportive of Glymphatic Function Impairment in Parkinson Disease. *Parkinsonism Relat Disord* (2021) 89:98–104. doi: 10.1016/j.parkreldis.2021.06.004

35. Yang G, Deng N, Liu Y, Gu Y, Yao X. Evaluation of Glymphatic System Using Diffusion MR Technique in T2DM Cases. *Front Hum Neurosci* (2020) 14:300. doi: 10.3389/fnhum.2020.00300